JACS
JOURNAL OF THE AMERICAN CHEMICAL SOCIETY

ARTICLE

pubs.acs.org/JACS

Clean Coupling of Unfunctionalized Porphyrins at Surfaces To Give Highly Oriented Organometallic Oligomers

Sam Haq,[†] Felix Hanke,[†] Matthew S. Dyer,[†] Mats Persson,[*,†,‡] Patrizia Iavicoli,[§] David B. Amabilino,[*,§] and Rasmita Raval[*,†]

[†]Surface Science Research Centre and Department of Chemistry, University of Liverpool, Liverpool L69 3BX, United Kingdom

[‡]Department of Applied Physics, Chalmers University of Technology, SE-412 96, Göteborg, Sweden

[§]Institut de Ciència de Materials de Barcelona (ICMAB−CSIC), Campus Universitari, 08193-Bellaterra, Catalonia, Spain

ABSTRACT: The direct coupling of complex, functional organic molecules at a surface is one of the outstanding challenges in the road map to future molecular devices. Equally demanding is to meet this challenge without recourse to additional functionalization of the molecular building blocks and via clean surface reactions that leave no surface contamination. Here, we demonstrate the directional coupling of unfunctionalized porphyrin molecules—large aromatic multifunctional building blocks—on a single crystal copper surface, which generates highly oriented one-dimensional organometallic macromolecular nanostructures (wires) in a reaction which generates gaseous hydrogen as the only byproduct. In situ scanning tunneling microscopy and temperature programmed desorption, supported by theoretical modeling, reveal that the process is driven by C−H bond scission and the incorporation of copper atoms in between the organic components to form a very stable organocopper oligomer comprising organometallic edge-to-edge porphyrin−Cu−porphyrin connections on the surface that are unprecedented in solution chemistry. The hydrogen generated during the reaction leaves the surface and, therefore, produces no surface contamination. A remarkable feature of the wires is their stability at high temperatures (up to 670 K) and their preference for 1D growth along a prescribed crystallographic direction of the surface. The on-surface formation of directional organometallic wires that link highly functional porphyrin cores via direct C−Cu−C bonds in a single-step synthesis is a new development in surface-based molecular systems and provides a versatile approach to create functional organic nanostructures at surfaces.

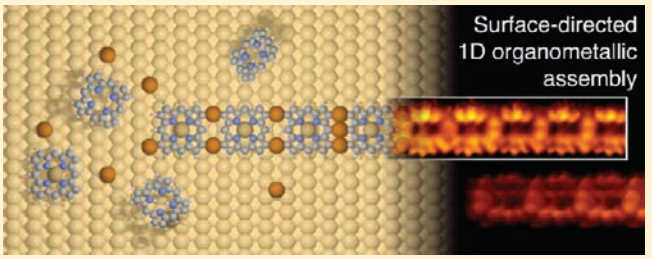

INTRODUCTION

The preparation of robust surface-based multimolecular nanostructures is a significant contemporary challenge, because of their potential as components of molecular electronic devices, molecular machines, optoelectronic devices, energy-harvesting systems, sensors, catalysts, molecular magnets, and smart coatings.[1−8] Given the major difficulties of transferring presynthesized complex macromolecules onto a surface in a controlled manner, the alternative bottom-up approach to fabricating macromolecular systems *directly* on a surface through surface-driven chemistry is a highly appealing prospect. To achieve this target, approaches to the generation of both covalent macromolecular[9−14] and coordination metal-molecule[15−22] systems have recently been demonstrated. However, most of this surface-confined chemistry has been directed by specific functionalization of the organic components, typically using halogenation or the incorporation of carboxylate, pyridyl, or carbonitrile functionalities. One significant exception is the direct covalent coupling of tetra-mesitylporphyrins on Cu(110),[10] which successfully created a rich diversity of oligo-porphyrin nanostructures and overcame the surface contamination problem arising from dehalogenation-based strategies. However, this system did not possess full directional control of the reaction. Therefore, although bottom-up surface chemistry represents a promising route to creating functional surface-based organic and metal−organic architectures, three key challenges currently remain to be tackled. First, is it possible to link the molecular units directly, without additional functionalization of the molecular building blocks, so that complex macromolecular chemistry can be realized in a simple manner at surfaces? Second, can such surface-driven molecular couplings be achieved via clean reactions, which do not generate byproduct that could contaminate the final product and the surface? Third, can a degree of directional control be attained in such systems where no spatially positioned connecting functional groups have been added?

Here, we show a system which fulfills all of these criteria whereby direct linking of the organic components is delivered in a single step at a surface via C−H bond scission and the formation of C−Cu−C organometallic bonds [15], to produce largely linear macromolecular porphyrin−metal organometallic wires which preferentially propagate along the [001] crystallographic direction of the surface. This reaction, summarized in Scheme 1, only generates hydrogen as a by-product, which is desorbed from the surface resulting in no surface contamination.

Received: February 14, 2011
Published: June 28, 2011

dx.doi.org/10.1021/ja201389u | *J. Am. Chem. Soc.* 2011, 133, 12031–12039

Scheme 1. Coupling Organic Components at Metal Surfaces via Direct Carbon−Metal Organometallic Bonds

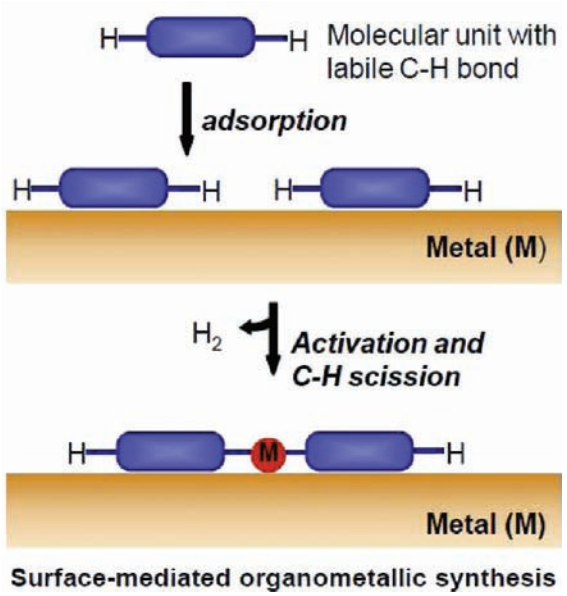

The ability to use the carbon−metal linkage that has been so powerful in organometallic chemistry to directly connect highly functional units such as porphyrins so that their rich operating capabilities can be transferred to a surface opens up new scientific and technological opportunities for surface-bound molecular devices. Significantly, the capability of tuning surface-anchored nanostructure properties via both the coordinating metal and the molecular functionality is now inherent in such surface-bound organometallic structures. Finally, the directional control exerted via structural matching of molecular architecture with the surface geometry provides new routes to engineering specific organic-based nanostructures at surfaces. Directionality and shape of nanostructures are often intimately related to function. Specifically, directional control of macromolecular structures is an important challenge for the transfer and processing of electrical and magnetic signals, and we anticipate that our approach will open up new strategies in this regard. Within the context of porphyrin-based systems, we note that 1D directly coupled porphyrin arrays, prepared by completely different oxidative coupling chemistry, have already shown remarkable electronic, photophysical, and electrochemical properties in solution.[23−26] Further, organometallic macromolecules are, in their own right, of general interest in photoactive, electroactive, and magnetic materials[27,28] and surface-driven chemistry of the type exemplified in this work provides an alternative to traditional solution-based approaches[29] and may open up connection regimes that have, thus far, been inaccessible.

METHODS

Experimental Details. STM experiments were performed under UHV conditions using a Specs STM 150 Aarhus instrument. The STM was calibrated to better than 5% accuracy by measuring the atomic distances of the clean Cu(110) surface. All measurements were taken in constant current mode, using a tungsten tip and at a base pressure of 1.5×10^{-10} mbar. Bias voltages are measured at the sample ($V = V_{sample}$). STM images were enhanced for brightness and contrast using the Image SxM program. In Figure 3a, low pass filtering was also used. The Cu(110) surface was prepared using Argon ion sputtering and annealing cycles, and atomic flatness and cleanliness were checked by STM and LEED prior to dosing the molecule. TPD spectra were collected between 273 and 800 K by heating the Cu(110) crystal at a rate of $\sim$2 K s^{-1} while measuring the change in partial pressure of mass 2, as a function of sample temperature. H_2−porphyrin and Cu−porphyrin (Frontier Scientific) were used as purchased and sublimed at $\sim$430 K onto the Cu(110) surface, which was held at room temperature during deposition. 5,15-Diphenylporphyrin was purchased from Frontier Scientific, and the Zinc(II) complex was synthesized by reaction with Zinc(II)acetate in dimethylformamide at 120 °C for 3 h. The mixture was cooled and water was added. The precipitate was filtered, washed with water and diethyl ether, and air-dried. The resulting material was chromatographed by flash column chromatography on silica using dichloromethane-hexane 4-6 as eluent. The product was further purified by crystallization from toluene. The product gave the characteristic spectroscopic data for this Zn(II)porphyrin,[30] with no indication of the free base porphyrin in the UV−visible spectrum, laser desorption-ionization mass spectrum, or in the ^{1}H NMR spectrum.

Computational Details. The density functional calculations were performed using the VASP code.[31] Plane waves were used as a basis set with an energy cutoff of 400 eV. Valence electron−core interactions were included using the projector augmented wave method[32] and the generalized gradient approximation (PW91) was used for the exchange-correlation functional.[33] The calculations of the periodic chain structures were carried out in a 3×6 surface unit cell using a $4 \times 3 \times 1$ k-point grid. The copper surface was modeled using a four layer slab, where the bottom two layers were fixed in their calculated bulk positions and the top two layers were allowed to relax. The vacuum separation between the copper slabs was 16.8 Å, leaving about 15 Å between the molecule and the back of the next slab. Adsorption and coupling geometries were calculated by placing a porphyrin molecule above the surface and allowing all molecular atoms and the top two layers of the copper slab to relax until all the forces on the atoms were less than 0.01 eV $Å^{-1}$. STM images were calculated in the Tersoff-Hamann approximation[34] using the implementation by Lorente and Persson.[35]

To study the adsorption process, calculations were performed for the full adsorbate−surface system, and also on the isolated molecular overlayer, the isolated Cu−porphyrin chains, the isolated radicals (e.g., chains without the Cu atoms), and the isolated copper substrate in the same calculation supercell. The adsorption energies were computed using:

$$E_{ads} = E_{sys} - E_{subs} - E_{Cu\text{-}P,\,vac} - n_{Cu}E_{Cu,\,ads} + 2n_{Cu}E_{H,\,ads} \quad (1)$$

where E_{sys} is the energy of the system, E_{subs} and $E_{Cu\text{-}P,vac}$ are the energies of the metal substrate and the Cu−porphyrin in vacuum, $E_{Cu,ads}$ and $E_{H,ads}$ are the energies of single adsorbed Cu and H-atoms, respectively, and n_{Cu} is the number of Cu adatoms (C−Cu−C couplings) per porphyrin molecule in the system. The bonding electron density in Figure 4 was visualized by obtaining the total density for the adsorbed Cu−porphyrin complex and subtracting the total electron density of the Cu slab (with the adatoms) and the radical.

RESULTS AND DISCUSSION

The organic multifunctional unit we have used in this work is the porphyrin molecule. This big family of compounds represents the central working unit in a wide variety of important applications[36−40] in both natural and technological systems such as oxygen-transport, light-harvesting, charge-separation, molecular data storage, sensory devices, photonic wires, field effect transistors, and light emitting diodes. The porphyrins chosen for

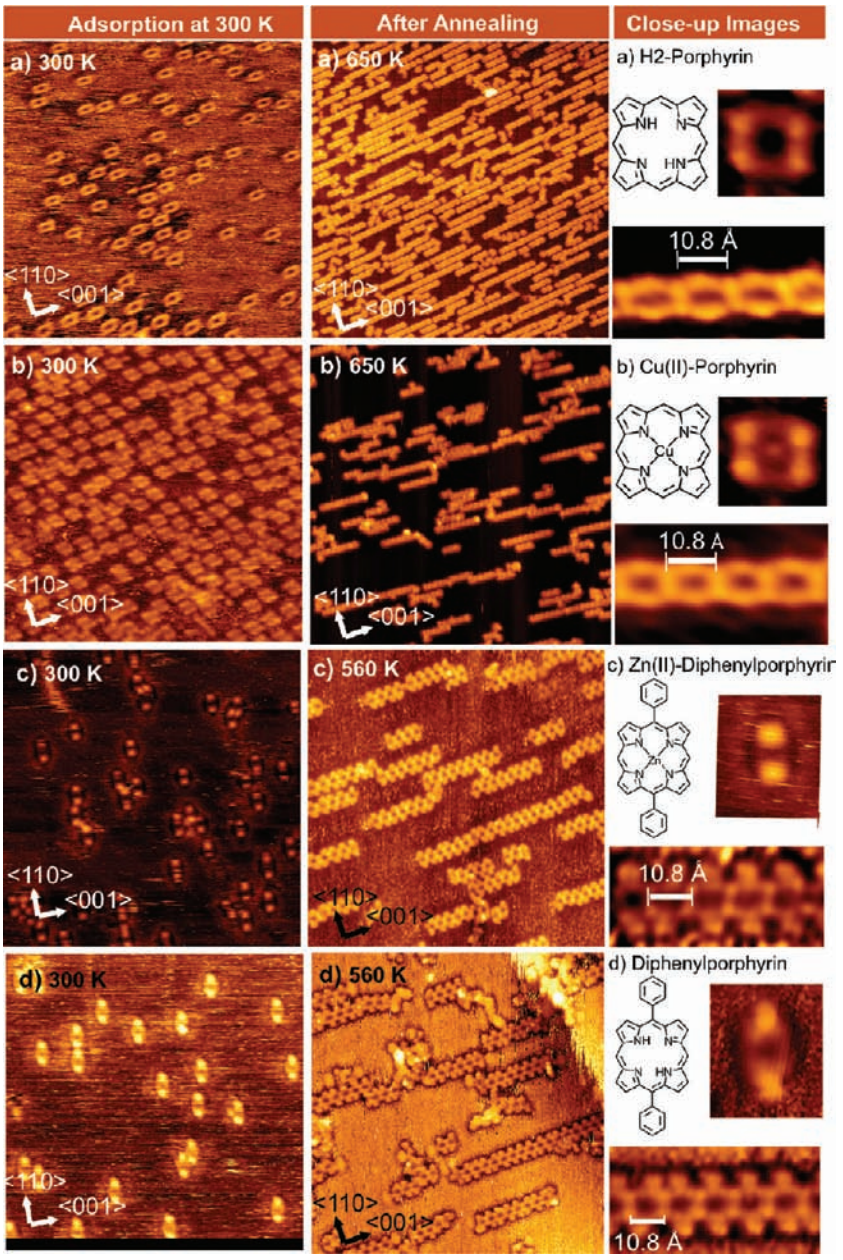

Figure 1. Scanning tunneling microscopy images showing the behavior of four different porphyrins on Cu(110) at room temperature (left column) and upon annealing (middle column). The room temperature and annealed images were recorded in separate experiments and do not represent the same porphyrin coverage. The molecular structure of the porphyrin and close up images of the room temperature isolated species and the macromolecular chains formed upon heating are also shown (right column). (a) H_2—porphyrin on Cu(110): (left) 20 nm × 20 nm STM image of adsorbed species at room temperature (V_t = −0.69 V, I_t = 0.29 nA); (middle) 60 nm × 60 nm STM image after annealing to 650 K (V_t = +0.30 V, I_t = 0.31 nA); (right, top) 1.68 nm × 1.80 nm STM image showing detail of the isolated species at room temperature and (right bottom) detail of the macromolecular chain formed upon annealing. (b) Cu(II)—porphyrin on Cu(110): (left) 20 nm × 20 nm STM image of adsorbed species at room temperature (V_t = −0.53 V, I_t = 0.39 nA); (middle) 62 nm × 62 nm STM image after annealing to 650 K (V_t = −0.69 V, I_t = 0.19 nA); (right, top) 1.75 nm × 1.8 nm STM image showing detail of the isolated species at room temperature and (right, bottom) detail of the macromolecular chain formed upon annealing. (c) Zn(II)—diphenyl porphyrin on Cu(110): (left) 20 nm × 20 nm STM image of adsorbed species at room temperature (V_t = −0.63 V, I_t = 0.18 nA); (middle) 30 nm × 30 nm STM image after annealing to 560 K (V_t = −1.03 V, I_t = 0.20 nA); (right, top) 2.6 nm × 3.0 nm STM image showing detail of the isolated species at room temperature and (right, bottom) detail of the macromolecular chain formed upon annealing. (d) Diphenyl porphyrin on Cu(110): (left) 20 nm × 20 nm STM image of adsorbed species at room temperature (V_t = −0.71 V, I_t = 0.33 nA); (middle) 28 nm × 28 nm STM image after annealing to 560 K (V_t = −1.68 V, I_t = 0.41 nA); (right, top) 2.3 nm × 3.0 nm STM image showing detail of the isolated species at room temperature and (right, bottom) detail of the macromolecular chain formed upon annealing.

this study were H_2—porphyrin and copper(II)—porphyrin, Figure 1, panels a and b, respectively, representing the free-base and metalated version of the tetrapyrrole macrocycle that is common to all porphyrins. In addition, 5,15-diphenyl porphyrin and zinc(II)-5,15-diphenyl porphyrin were also studied to help locate the site of the coupling, with the two phenyl groups acting

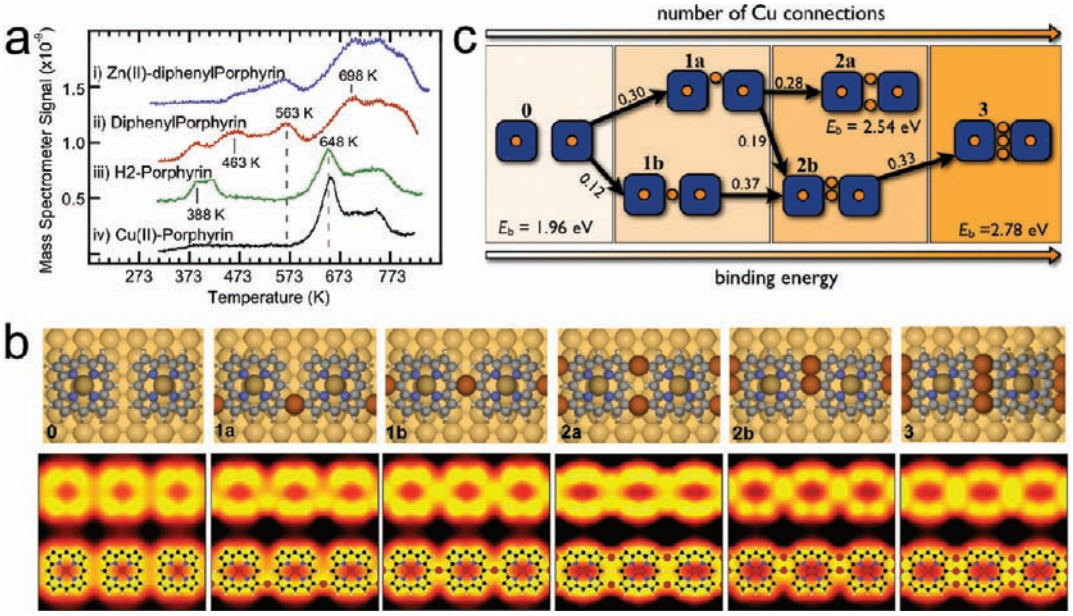

Figure 2. Hydrogen evolution, energetics and structures associated with the porphyrin−metal coupling reactions. (a) Temperature Programmed Desorption curves obtained for porphyrins on Cu(110), showing the evolution of hydrogen (amu = 2) upon increasing temperature, corresponding to: metalation of the porphyrin ring of (ii) and (iii) between at 360−420 K; C−H bond breaking to form porphyrin−Cu−porphyrin linkages between 420 and 590 K for (i) to (ii) and between 600 and 670 K for (iii) and (iv); and, finally, to decomposition of the molecules at the surfaces. (b) Calculated geometries (top) and simulated STM images (bottom) for the six distinct porphyrin linkages formed by Cu−porphyrin containing zero, one, two, or three connecting Cu atoms. Each modeled STM image (3.27×3.08 nm^2) corresponds to the geometry shown above and was calculated for a sample bias of −0.82 V. For the connections **1a**, **1b**, and **2a**, one can clearly distinguish separate protrusions for each Cu atom while the **2b** and **3** connections show elongated protrusions that traverse neighboring copper atoms. Each connection can be uniquely identified by the number of protrusions and their location with respect to the porphyrin macrocycle. (c) Computed reaction energies for the Cu−porphyrin linking process showing the exothermic nature of each separate linking reaction. The binding energy increases from left to right. The net adsorption energies are shown for the initial configuration **0** and the two terminal connections **2a** and **3**.

as markers of molecular geometry for the microscopy studies, Figure 1c,d.

When each of the four porphyrins is sublimed onto the Cu(110) surface in ultrahigh vacuum (UHV) at room temperature and imaged by scanning tunneling microscopy (STM), the adsorbed molecules appear as isolated single species at the surface, Figure 1. The H_2−porphyrin and Cu−porphyrin image as square-shaped protrusions, which are attributed to individual molecules adsorbed at the Cu(110) surface. In contrast, the diphenyl porphyrins image as oval-shaped single species characterized by two bright lobes at opposite extremes, which are all oriented parallel to the main Cu[1$\bar{1}$0] symmetry axis that coincides with the close-packed Cu rows on the surface. The size of the oval images is 1.5 nm × 0.8 nm which is consistent with the size of the diphenyl porphyrins and the two bright lobes can be attributed to the two phenyl substituents on the porphyrin ring. At room temperature, all four adsorbed porphyrin molecules remain as discrete species and there are no permanent connections formed between the molecules.

When either H_2−porphyrin or copper(II)−porphyrin were heated to 650 K on the metallic copper surface, the resulting STM images obtained after cooling the surface to room temperature show that, during the heating, long and regular macromolecular chains, up to 12 units long, have been formed that run parallel to the [001] symmetry axis of the surface (Figure 1a,b). Similarly, when 5,15-diphenyl porphyrin and Zn(II)-5,15-diphenyl porphyrin are heated to 560 K on Cu(110), we observe that a similar coupling also occurs and STM images show long macromolecular structures are now formed at the surface (Figure 1c,d). Detailed STM images for all four systems show an area of bright contrast at the junction of adjacent porphyrin cores and all display a repeat core-to-core distance of 10.8 Å between the coupled porphyrins, suggesting a common linking scheme. Specifically, the phenyl groups at the 5,15 positions of the diphenyl porphyrins are imaged distinctly in small-area STM images (Figure 1c,d) and show unambiguously that the linkage occurs directly between the macrocycles' peripheries, linking each carbon edge to that of the adjacent molecule. This clear linkage preference, combined with the highly preferred molecular orientation on the surface, forces the linked 1D macromolecular structures to propagate predominantly along the [001] direction of the copper surface. We note, however, that within this generally adopted orientation, a small proportion of local irregularities within the linked structures are also seen, with a slight displacement observed between adjacent porphyrins and, on occasion, a twist between adjacent tetrapyrrolic cores. These observations suggest that, although the intermolecular connection always occurs directly between the macrocycles, a number of different kinds of links can potentially be formed during the reaction.

Temperature Programmed Desorption (TPD) experiments provide further insight into the process that leads to the on-surface coupling of the porphyrins. It is instructive to analyze this data by considering the porphyrins and the diphenyl porphyrins separately. When 5,15-diphenyl porphyrin is heated on the copper surface, TPD experiments (Figure 2a(ii)) show hydrogen desorption between 360 and 410 K, indicating the transformation of diphenyl porphyrin to Cu−diphenyl porphyrin, corresponding

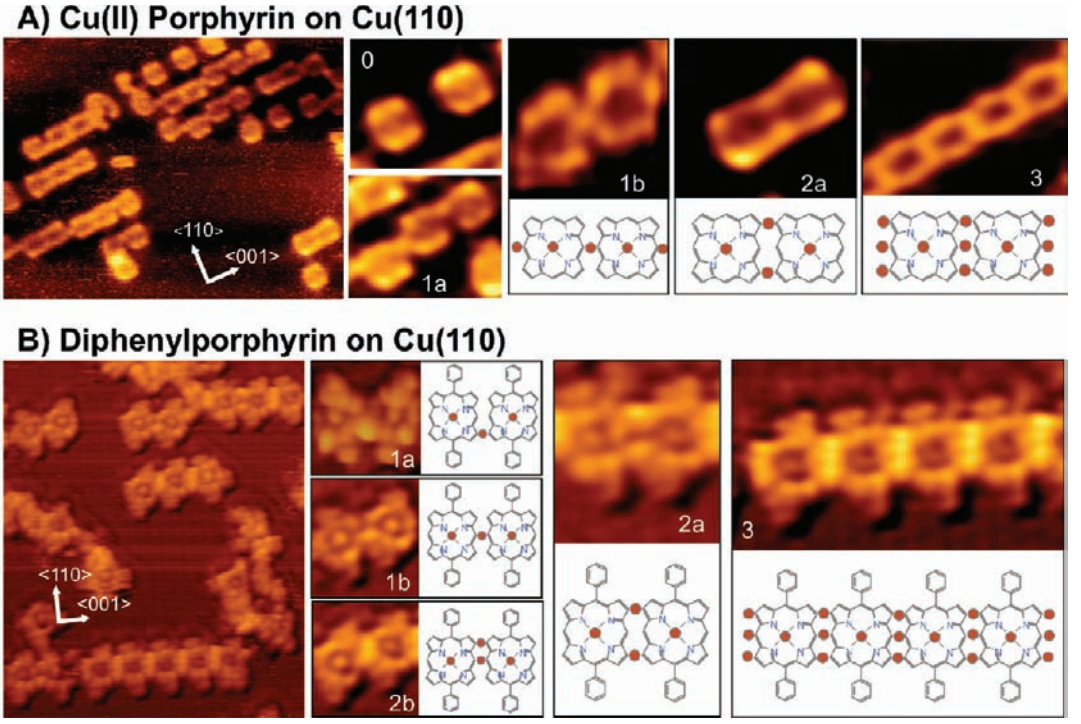

Figure 3. STM images showing that a variety of porphyrin−Cu−porphyrin connections are observed at the onset of the coupling reaction. Schematic models are shown for a range of observed connections that should generate 1D oriented organometallic oligomers. (a) Cu−porphyrin on Cu(110): (left) large area STM 15.0 nm × 11.5 nm (V_t = −0.82 V, I_t = 0.3 nA) showing a variety of coupled Cu−porphyrin entities at the surface following annealing treatment to ∼620 K, with (right) examples of the **0**, **1a**, **1b**, **2a**, and **3** connections shown in detail alongside. The crystallographic directions shown in the main picture apply to the other images. (b) Diphenyl porphyrin on Cu(110): (left) large area STM 10 nm × 8 nm (V_t = +0.17 V, I_t = 0.23 nA) showing a variety of coupled diphenyl porphyrin entities at the surface following annealing treatment to 460 K, with (right) examples of the **0**, **1a**, **1b**, **2a**, **2b**, and **3** connections shown in detail alongside. The crystallographic directions shown in the main picture apply to the other images.

to N−H bond scission and incorporation of the metal into the center of the porphyrin ring, as reported in a related system.[10] As expected, there is no corresponding metalation-induced hydrogen evolution in this temperature range for the Zinc(II) diphenyl porphyrin, Figure 2a(i). When both diphenyl porphyrin systems are further heated up to between 420 and 590 K, evolution of hydrogen is observed across this temperature range, culminating in the long chain structures observed in the STM data shown in Figure 1c,d. Above 600 K, decomposition of the molecule commences. Turning to the H_2−porphyrin and copper(II)−porphyrin systems, it can be seen that Cu metalation of the porphyrin core is also observed for the former at 360−420 K, accompanied by H_2 evolution in the TPD. As expected, the copper(II)−porphyrin system shows no hydrogen evolution in this temperature range. Further heating to between 600 and 670 K is accompanied by hydrogen evolution that leaves Cu−porphyrin macromolecular chains at the surface for both systems.

There are two main facts that emerge from the TPD data. First, for both free base porphyrins, N−H bond scission and metalation of the porphyrin core occurs during the heating process at between 360 and 410 K. However, no coupling of the molecules is observed at this stage. Instead, coupling occurs at much higher temperatures (between 420 and 590 K for the diphenyl porphyrins and between 600 and 670 K for the native porphyrins) and is associated with further hydrogen evolution, which must correspond to C−H bond scission. Given that the site of the coupling can be identified to be at the edges of the porphyrins, two main possibilities may be suggested, namely, that coupling occurs via a direct C−C covalent linking of the macrocycles, or that it occurs via an organometallic coupling forming a C−Cu−C link. These two possibilities can be easily distinguished by measuring the distances between the coupled porphyrin cores, with the distances calculated for a gas-phase C−C covalently coupled oligomer to be 8.9 Å while an organometallic coupling would yield a distance of 10.9 Å. It is clear that our experimentally measured core-to-core distance of 10.8 Å agrees very closely with the formation of organometallic porphyrin−Cu chains. Thus, the observed macromolecular chains can be rationalized in terms of C−Cu−C coupling, and a number of connections can be postulated involving the formation of one, two, or three organometallic bonds at the 3, 5, and 7 positions of the porphyrin core that would link the peripheries of the molecules in the manner observed experimentally, as depicted in Figure 2b,c.

The copper incorporation into the cores of the porphyrin and diphenyl porphyrin systems takes place at a similar temperature presumably because the reactivity of the nitrogen atoms remains unaffected by the diphenyl substitution. This behavior is consistent with work showing that the electron density in the HOMO of the two macrocycles at these positions is similar.[41] In contrast, our experimental data shows that the reactivity of the C−H groups at the meso and beta positions of the porphyrins is enhanced by the diphenyl substituents, with C−H bond scission occurring at a lower temperature. This may be attributed to the fact that the incorporation of phenyl substituents onto the porphyrin core modifies the electronic properties of the macrocycle.[41−43] Further, there is no observation of phenyl group reactivity for the diphenyl porphyrins and this may be

rationalized on the basis that the HOMO and LUMO of these porphyrins possess most density at the pyrrole rings rather than the phenyl substituents,[43] implying that the pK_a values of the phenyl protons must be significantly higher than those of the heterocycle, providing selectivity in the chemistry even at high temperatures.

To understand the structure of the regular [porphyrin−Cu]$_n$ chains formed at the surface and the thermodynamic factors that drive this organometallic assembly, density functional calculations were undertaken for the Cu−porphyrin system. The relaxed structures for surface-bound organometallic chains possessing all of the possible Cu−porphyrin connections are shown in Figure 2b, ranging from two distinct 1-connection linkages (**1a**, **1b**), two distinct 2-connection linkages (**2a**, **2b**), and one unique 3-connection linkage (**3**). In all cases, the Cu−porphyrin moiety occupies an adsorption position in which the central Cu atom is located at a short-bridged site on top of the Cu metal rows. This adsorption geometry was also shown to be favored for the free-base porphyrin molecule[44] and the Co-tetraphenylporphyrin[45] molecules on this surface. Uniquely, this enables the connecting Cu atoms at the peripheries to occupy their strongly preferred 4-fold coordinated hollow sites between the close-packed [1$\bar{1}$0] rows of the Cu surface. The lowest energy chain structures computed for the different organometallic connections are shown in Figure 2b and all possess a porphyrin−porphyrin core distance of 10.9 Å, which is close to that observed experimentally. The Cu−C distance calculated for the organometallic connections average at 1.95 ± 0.02 Å, with a slightly shorter bond-length average of 1.93 Å being observed for the Cu−C bonds forming the top and bottom connections, while the middle Cu−C connection possesses a longer bond length average of 1.98 Å.

STM simulations of the calculated 1-, 2-, and 3-Cu organometallic chain structures formed from copper−porphyrin units are also shown in Figure 2b and reveal that the connecting Cu atoms image as bright protrusions at the junction between the molecules and that the various linkages can, in principle, be distinguished by the location and nature of these bright features. In fact, all possible connections suggested in Figure 2b were observed experimentally at the earliest stage of the reaction. Figure 3 shows STM data collected for the copper(II) porphyrin and diphenyl porphyrin systems, captured at the onset of the coupling reaction when the systems are heated to intermediate temperature. These images indeed reveal that a variety of coupling connections can be captured from 1-Cu to 3-Cu connections, with identification made possible from comparing simulated STM images (Figure 2b) to the experimental results (Figure 3).

The calculated energies associated with the formation of 1-, 2-, and 3-connection chains show that a significant thermodynamic advantage results from C−H bond breaking and incorporation of a Cu atom to make the C−Cu−C connection. Figure 2c shows that the creation of a porphyrin chain with a 1-Cu connection is associated with a 0.12 or 0.3 eV energy gain, depending on the location of the connection. The incorporation of further Cu atoms always results in energy gains of between 0.19 and 0.37 eV per porphyrin core, that is, when going from structure **1a** to **2a** or from **1b** to **2b** or from either **2a**/**b** to **3**. These results clearly show that a strong energetic driving force exists for the formation of organometallic porphyrin chains on the Cu(110) surface.

We note that the **1a** and **2b** connection coupling schemes could lead to slightly irregular structures in which adjacent porphyrins are displaced, twisted, or kinked with respect to each

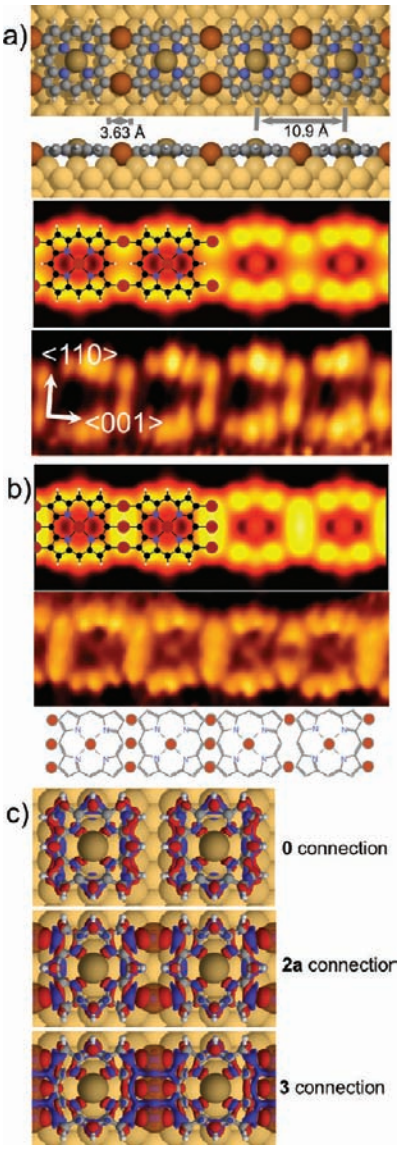

Figure 4. The nature of the Cu−porphyrin chain formed at the surface with a **2a** and a **3** connection. (a) (Top): Computed geometric structure of the Cu−porphyrin chain with connection **2a** presenting top- and side-views showing the length scale and the bending of the porphyrin macrocycle toward the two connecting Cu atoms; (middle) simulated STM images (4.36 nm × 1.54 nm, V_{tip} = −0.1 V) and (bottom) experimental STM image 4.45 nm × 1.4 nm (V_t= +0.4 V, I_t = 0.42 nA) showing submolecular detail of a **2a** coupled Cu−porphyrin nanowire. (b) (Top): Simulated STM images (4.36 nm × 1.54 nm, V_{tip} = −0.1 V) of a Cu−porphyrin nanowire with a **3** connection; (middle) experimental STM image 4.60 nm × 1.4 nm (V_t= −0.76 V, I_t = 0.19 nA) showing submolecular detail of a Cu−porphyrin nanowire with predominantly **3** connections and one **2a** connection with (bottom) showing a schematic representation identifying each connection. (c) Calculated electron density differences for connection **0** (top), the **2a** connection (middle) and the **3** connection (bottom) indicating the bonding mechanisms for the C−Cu−C connection and the Cu−porphyrin−substrate interaction. The electron density difference is taken between the adsorbed system and the bare surface and the isolated Cu−porphyrin molecule (connection **0**) and the radical (connection **2a**). Red and blue correspond to electron accumulation and depletion, respectively. Note that the connecting Cu atoms are partially transparent for clarity.

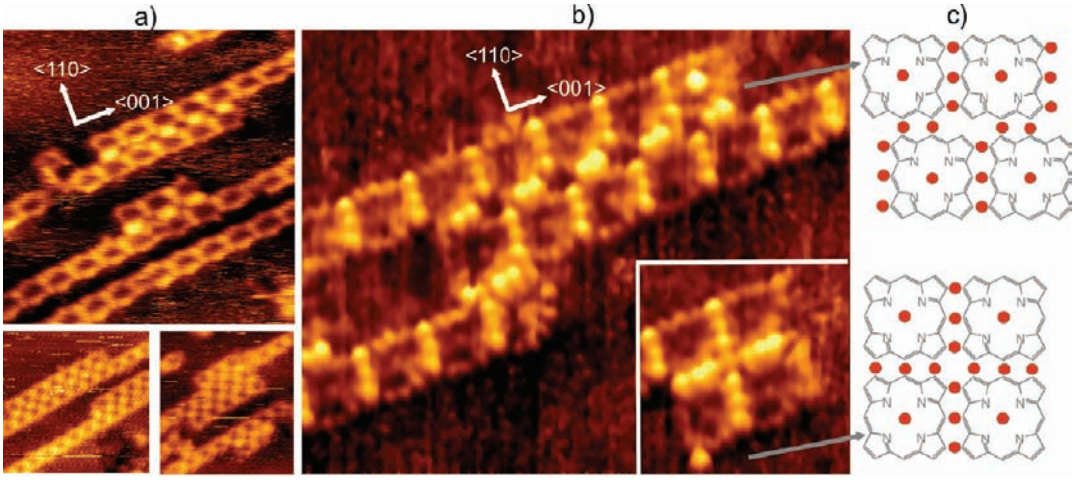

Figure 5. Extending the organometallic linkage to connect adjacent porphyrin chains. (a) Experimental STM images showing the formation of nanoribbons in which adjacent [porphyrin−Cu]$_n$ chains link together in the [1$\bar{1}$0] direction to make nanoribbons. Main image 10 nm × 10 nm (V_t = +0.07 V, I_t = 0.36 nA); top right image 10.2 × 9.8 nm (V_t= +0.51 V, I_t = 0.3 nA) ; bottom right image 9 nm × 9.5 nm (V_t= +0.51 V, I_t = 0.3 nA). (b) Experimental STM images revealing the incorporation of Cu atoms between adjacent porphyrin chains leading to nanoribbon formation with staggered arrangements or to aligned structures such as the tetramer shown in the inset. Main image 8.7 nm × 6.5 nm (V_t = −0.67 V, I_t = 0.30 nA); inset image 2.8 × 2.8 nm (V_t= −0.67 V, I_t = 0.30 nA). (c) Schematic drawings showing the repeat unit of the nanoribbon and the tetramer imaged in (b).

other, as observed experimentally in Figure 3 during the onset of coupling. In contrast, the **3** three-bond coupling and the **1b** and **2a** two-connection linkages would all lead to a highly defined 1-D linear conformation. The energy hierarchy depicted in Figure 2c would predict the following mechanistic route: **0** → **1a** → **2a**. The final step from **2a** to **3** would either require reorganization of the already-formed Cu−C connections to allow the third Cu atom to be incorporated, or a mechanism that would involve diffusion of the third Cu atom into the central position.

Experimentally, we observe that once the porphyrin systems have been subject to higher temperatures, the formation of longer and straighter chains occur in which the **2a** and **3** connection schemes predominate, Figures 1 and 3. Further information on the nature of the highly linear chains is obtained from detailed examination of the Cu−porphyrin system. The computed geometries and STM simulations of a **2a** connection chain is shown in Figure 4a. The experimental STM image of a chain formed solely from **2a** connections is also displayed in Figure 4a and it can be seen that the experimental data are in very good agreement with the **2a** coupling scheme shown where Cu insertion has occurred at the 3 and 7 positions. Both theory and experiment show a three-petal STM structure at the top and bottom edge of the porphyrin ring. In addition, the bright two-lobed hourglass structure imaged experimentally at the junction of the porphyrins is only consistent with the 2-Cu coupling shown in **2a**. Figure 4b displays an experimental STM image in which a linear chain with predominantly **3** connections is observed. Again, a good agreement with the simulated STM image is obtained, with the three petal structure also present at the top and bottom edge of the porphyrin and the **3** Cu connection imaging as an elongated strip of brightness, consistent with the incorporation of Cu at the 3, 5, and 7 positions. The single **2a** connection within this chain is also readily identifiable with the two connecting Cu atoms imaging as two discrete spots. This allows a schematic, which pinpoints each individual connection, to be drawn for this chain as shown at the bottom in Figure 4b.

The nature of the chemical bond of the C−Cu−C connection in the Cu−porphyrin chain is revealed by plotting the electron density differences for the nonconnected system, the **2a** connection system and the **3** connected chain, shown in Figure 4c. The electron density rearrangements around the C−Cu−C connection show that the electron density is enhanced between the atoms in the connections and leads to the formation of local C−Cu organometallic bonds. The shape of this density shows that these bonds are covalent σ bonds involving sp^2 states of the C atoms and d states of the Cu atom.

Finally, we note that with relatively high molecular coverage at the surface and slow annealing treatments to ∼670 K, we were also able to extend the organometallic coupling into the orthogonal [1$\bar{1}$0] direction to yield nanoribbons in which two or three adjacent chains of porphyrins are connected, Figure 5a, with the junctions imaging brightly, suggesting the incorporation of metal atoms between the adjacent chains. This is confirmed by STM images obtained under rare tip conditions in which the connecting Cu atoms were imaged clearly and which reveal that adjacent chains can be either staggered by one connection with respect to each other or be completely aligned, Figure 5b,c. Thus, organometallic ribbons and, occasionally, localized architectures such as highly regular tetramers are generated. However, we point out that the creation of ribbons that are 2 and 3 porphyrin units wide is a much rarer event than growth propagation along the [001] direction and the formation of localized aligned tetramer structures as shown in Figure 5c is even scarcer, suggesting that their formation is highly hindered.

■ CONCLUSIONS

We have demonstrated that surface-driven chemistry using unfunctionalized aromatic molecules can be used for the efficient formation of pure organometallic wires one molecule wide at a surface, in which the alternate incorporation of highly conjugated organic and metallic subunits occurs at the nanometer scale along a preferred crystallographic direction. A strong energetic driving force exists for the formation of these oriented organometallic porphyrin chains on the surface. This finding opens up the prospect of using the highly versatile organometallic linkage to

directly couple complex organic units at surface without having to introduce additional functionalities to forge the metal−molecule connections. Additionally, the demonstration that directional control can be wielded via structural matching of molecular geometry to the surface dimensions provides potentially new routes to engineering oriented molecular nanostructures at surfaces. The organometallic arrays created here deliver robust and linearly organized catalytic, sensing, and magnetic templates onto a surface. Further, the capability of dual-tuning these functions, via both the metal and the molecular functionality, are now inherent in such surface-bound organometallic structures. Finally, the surface chemistry demonstrated here only requires the C−H bond to be ruptured, meaning minimum precursor modification, and only generates gaseous H_2 resulting in minimum surface contamination.

Linearly linked porphyrin tapes have been shown to possess important properties for molecular electronics, dyes, sensors, and nonlinear optics[23−26] in the solution phase and it may be anticipated that the 1D organometallic wires created in this work may translate such potential to surface-based systems. In a wider context, we also point out that the surface chemistry reported here represents new reaction pathways that have no analogue in solid or solution-phase chemistry. For example, achieving a pure C−Cu organocopper linkage to create macromolecular structures is generally not easily realized and, in solution, aryl copper compounds are most frequently prepared by reactions of copper(I) salts with other organometallic compounds (habitually based on lithium or magnesium). To our knowledge, there is no precedent of the copper-linkage chemistry shown here in solution based organometallic systems. Thus, the direct formation of organocopper species in a single-step from copper metal and the nonactivated aromatic raises new perspectives for the development of synthetic routes for organometallic materials. Additionally, the edge-to-edge organometallic linkage reported here is unprecedented for porphyrin-based macromolecules, and opens up new possibilities in this area of materials science. In this respect, the thermal stability of the macromolecular fibres is promising for technological application. The present results are also relevant in the context of recent interest in C−H functionalization in organic synthesis[46] and may also illuminate new pathways for preparing compounds from the parent polypyrrole porphyrin macrocycle, which has attracted recent interest.[47]

AUTHOR INFORMATION

Corresponding Author

mpersson@liv.ac.uk; amabilino@icmab.es; raval@liv.ac.uk

ACKNOWLEDGMENT

The research was supported by the UK EPSRC grant EP/F00981X/1 for R.R., the MICINN (CTQ2010-16339) and the Generalitat de Catalunya (2009 SGR 158) for D.B.A., the EU project ARTIST (grant agreement no. 243421) for F.H. and M.P. and the Swedish Research Council (VR) for M.P., and the University of Liverpool for M.S.D.

REFERENCES

(1) Maruccio, G.; Cingolani, R.; Rinaldi, R. *J. Mater. Chem.* **2004**, *14*, 542–554.

(2) Scheybal, A.; Ramsvik, T.; Bertschinger, R.; Putero, M.; Nolting, F.; Jung, T. A. *Chem. Phys. Lett.* **2005**, *411*, 214–220.

(3) Rapenne, G.; Launay, J. P.; Joachim, C. *J. Phys.: Condens. Matter* **2006**, *18*, S1797–S1808.

(4) Shirai, Y.; Morin, J. F.; Sasaki, T.; Guerrero, J. M.; Tour, J. M. *Chem. Soc. Rev.* **2006**, *35*, 1043–1055.

(5) Kim, W. Y.; Choi, Y. C.; Kim, K. S. *J. Mater. Chem.* **2008**, *18*, 4510–4521.

(6) Diez-Perez, I.; Hihath, J.; Lee, Y.; Yu, L. P.; Adamska, L.; Kozhushner, M. A.; Oleynik, I. I.; Tao, N. J. *Nat. Chem.* **2009**, *1*, 635–641.

(7) Mannini, M.; Pineider, F.; Sainctavit, P.; Danieli, C.; Otero, E.; Sciancalepore, C.; Talarico, A. M.; Arrio, M. A.; Cornia, A.; Gatteschi, D.; Sessoli, R. *Nat. Mater.* **2009**, *8*, 194–197.

(8) Lobo-Checa, J.; Matena, M.; Müller, K.; Dil, J. H.; Meier, F.; Osterwalder, J.; Gade, L. H.; Jung, T. A.; Stöhr, M. *Science* **2009**, *325*, 300–303.

(9) Grill, L.; Dyer, M.; Lafferentz, L.; Persson, M.; Peters, M. V.; Hecht, S. *Nat. Nanotechnol.* **2007**, *2*, 687–691.

(10) In't Veld, M.; Iavicoli, P.; Haq, S.; Amabilino, D. B.; Raval, R. *Chem. Commun.* **2008**, 1536–1538.

(11) Weigelt, S.; Busse, C.; Bombis, C.; Knudsen, M. M.; Gothelf, K. V.; Lægsgaard, E.; Besenbacher, F.; Linderoth, T. R. *Angew. Chem., Int. Ed.* **2008**, *47*, 4406–4410.

(12) Lipton-Duffin, J. A.; Ivasenko, O.; Perepichka, D. F.; Rosei, F. *Small* **2009**, *5*, 592–597.

(13) Cai, J.; Ruffieux, P.; Jaafar, R.; Bieri, M.; Braun, T.; Blankenburg, S.; Muoth, M.; Seitsonen, A. P.; Saleh, M.; Feng, X.; Mullen, K.; Fasel, R. *Nature* **2010**, *466*, 470–473.

(14) Matena, M.; Stöhr, M.; Riehm, T.; Björk, J.; Martens, S.; Dyer, M. S.; Persson, M.; Lobo-Checa, J.; Müller, K.; Enache, M.; Wadepohl, H.; Zegenhagen, J.; Jung, T. A.; Gade, L. H. *Chem.—Eur. J.* **2010**, *16*, 2079–2091.

(15) We note that the terms 'organometallic compound' and 'coordination-metal compounds' are often used interchangeably in the surface science literature. In this paper, we utilize the formal definition of organometallic as only referring to compounds containing carbon−metal bonds, while metal-coordination compounds refer to metal connections with other (hetero)atoms (notably N, O, etc.).

(16) Classen, T.; Lingenfelder, M.; Wang, Y.; Chopra, R.; Virojanadara, C.; Starke, U.; Costantini, G.; Fratesi, G.; Fabris, S.; de Gironcoli, S.; Baroni, S.; Haq, S.; Raval, R.; Kern, K. *J. Phys. Chem. A* **2007**, *111*, 12589–12603.

(17) Heim, D.; Seufert, K.; Auwärter, W.; Aurisicchio, C.; Fabbro, C.; Bonifazi, D.; Barth, J. V. *Nano Lett.* **2009**, *10*, 122–128.

(18) Fendt, L.-A.; Stöhr, M.; Wintjes, N.; Enache, M.; Jung, T. A.; Diederich, F. *Chem.—Eur. J.* **2009**, *15*, 11139–11150.

(19) Heim, D.; Écija, D.; Seufert, K.; Auwärter, W.; Aurisicchio, C.; Fabbro, C.; Bonifazi, D.; Barth, J. V. *J. Am. Chem. Soc.* **2010**, *132*, 6783–6790.

(20) Marschall, M.; Reichert, J.; Weber-Bargioni, A.; Seufert, K.; Auwarter, W.; Klyatskaya, S.; Zoppellaro, G.; Ruben, M.; Barth, J. V. *Nat. Chem.* **2010**, *2*, 131–137.

(21) Liljeroth, P.; Swart, I.; Paavilainen, S.; Repp, J.; Meyer, G. *Nano Lett.* **2010**, *10*, 2475–2479.

(22) Bartels, L. *Nat. Chem.* **2010**, *2*, 87–95.

(23) Osuka, A.; Shimidzu, H. *Angew. Chem., Int. Ed. Engl.* **1997**, *36*, 135–137.

(24) Tsuda, A.; Furuta, H.; Osuka, A. *J. Am. Chem. Soc.* **2001**, *123*, 10304–10321.

(25) Tsuda, A.; Osuka, A. *Science* **2001**, *293*, 79–82.

(26) Kim, D; Osuka, A. *Acc. Chem. Res.* **2004**, *37*, 735–745.

(27) Abd-El-Aziz, S.; Shipman, P. O.; Boden, B. N.; McNeil, W. S. *Prog. Polym. Sci.* **2010**, *35*, 714–836.

(28) Hornig, S.; Manners, I.; Newkome, G. R.; Schubert, U. S. *Macromol. Rapid Commun.* **2010**, *31*, 771–771.

(29) Krause, N., Ed.; *Modern Organocopper Chemistry*: Wiley-VCH: Weinheim, Germany, 2002.

(30) Lin, V. S. Y.; Iovine, P. M.; DiMagno, S. G.; Therien, M. J. *Org. Synth.* **2002**, *33*, 55–61.

(31) Kresse, G.; Furthmüller, J. *Phys. Rev. B* **1996**, *54*, 11169.
(32) Kresse, G.; Joubert, D. *Phys. Rev. B* **1999**, *59*, 1758.
(33) Perdew, J. P.; Chevary, J. A.; Vosko, S. H.; Jackson, K. A.; Pederson, M. R.; Singh, D. J.; Fiolhais, C. *Phys. Rev. B* **1992**, *46*, 6671.
(34) Tersoff, J.; Hamann, D. R. *Phys. Rev. Lett.* **1983**, *50*, 1998.
(35) Lorente, N.; Persson, M. *Faraday Discuss.* **2000**, *117*, 277.
(36) Lindsey, J. S. *Acc. Chem. Res.* **2010**, *43*, 300–311.
(37) Severance, S.; Hamza, I. *Chem. Rev.* **2009**, *109*, 4596–4616.
(38) Mohnani, S.; Bonifazi, D. *Coord. Chem. Rev.* **2010**, *254*, 2342–2362.
(39) Di Natale, C.; Monti, D.; Paolesse, R. *Mater. Today* **2010**, *13*, 37–43.
(40) Latter, M. J.; Langford, S. J. *Int. J. Mol. Sci.* **2010**, *11*, 1878–1887.
(41) Gassman, P. G.; Ghosh, A.; Almlöf, J. *J. Am. Chem. Soc.* **1992**, *114*, 9990–10000.
(42) Schlözer, R.; Fuhrhop, J.-H. *Angew. Chem., Int. Ed. Engl.* **1975**, *14*, 363.
(43) Cramariuc, O.; Hukka, T. I.; Rantala, T. P. *Chem. Phys.* **2004**, *305*, 13–26.
(44) Dyer, M. S.; Robin, A.; Haq, S.; Raval, R.; Persson, M.; Klimes, J. *ACS Nano* **2011**, *5*, 1831–1838.
(45) Donovan, P.; Robin, A.; Dyer, M. S.; Persson, M.; Raval, R. *Chem.—Eur. J.* **2010**, *16*, 11641–11652.
(46) Davies, H. M. L.; Du Bois, J.; Yu, J. Q. *Chem. Soc. Rev.* **2011**, *40*, 1855–1856.
(47) Senge, M. O.; Davis, M. *J. Porphyrins Phthalocyanines* **2010**, *14*, 557–567.